ORIGINAL PAPER

Fracture analysis of a centrifugal ore slurry pump shaft: a study using fatigue tests, microstructural analysis and finite element simulation

J. C. de Lacerda[1] · R. L. P. Teixeira[1] · W. D. dos Reis[1] · A. S. T. Garcia[1] · T. G. de Brito[1] · R. F. Brito[1]

Abstract

Failures in centrifugal pump shafts used in ore slurry applications can cause significant downtime in mining operations. However, limited studies focus on the comprehensive analysis of such failures, particularly in terms of fatigue behavior, microstructure, and stress distribution. This study investigates the fracture failure of an AISI 4140 steel shaft from a centrifugal ore slurry pump used by a large mining company in Brazil. The research includes chemical and microstructural analyses, as well as mechanical tests (tensile, hardness, impact, and fatigue), with numerical simulations conducted under defined boundary conditions: torque of 3885 Nm and shaft support through two rolling bearings. Results revealed that fatigue nucleation occurred at multiple stress concentration points in the threaded region, leading to final fracture. The maximum equivalent stress was quantified as 203.57 MPa, consistent with the simulation results. The shaft's coarse bainitic microstructure reduced impact toughness, with a measured impact energy of 9 ± 2 J, while the fatigue limit was determined to be approximately 350 MPa.

Abbreviations

OES	Optical emission spectrometer
HR_C	Rockwell "C" hardness tests
da/dN	Crack growth (m/cycle)
R	Load ratio
ΔK	Stress intensity fator variation (MPa m$^{1/2}$)
SEM	Scanning electron microscopy
PSBs	Persistent slipping bands

1 Introduction

Centrifugal pumps play a crucial role in the mining industry, particularly in the transportation of ore slurry during mineral processing. These pumps are fundamental to the efficiency and productivity of mining operations, as they ensure the continuous flow of materials throughout the processing plant.

Any failure in these pumps, especially in their critical components such as the shaft, can result in significant operational downtime, financial losses, and safety risks. Understanding the factors that lead to shaft failures is essential for improving pump reliability and minimizing unexpected production stoppages.

Recent research emphasizes the need to understand how mechanical stress, microstructure, and material properties collectively affect shaft fatigue (Liu et al. 2019; Anderson 2017). However, comprehensive studies that integrate experimental testing and finite element analysis under realistic conditions remain limited (Meysami et al. 2010; Bhadeshia & Honeycombe 2017). This study aims to bridge this gap by examining fatigue, microstructural characteristics, and stress distribution in centrifugal pump shafts, providing both theoretical insights and practical recommendations for improved maintenance strategies.

1.1 Context of iron ore processing

The processing of iron ores involves various physical and chemical operations to prepare the material for steel production. These operations include comminution, classification, and concentration, among others. Centrifugal pumps are essential in wet processing, as they transfer ore slurry

✉ J. C. de Lacerda
jlacerda@unifei.edu.br

1 Federal University of Itajubá - Itabira Campus, Itabira, MG 35903-087, Brazil

throughout the stages of separation, impacting the overall efficiency of the plant (Rodrigues 2023).

1.2 Importance of centrifugal pump shafts

Centrifugal pumps consist of several components, with the shaft being critical for torque transmission from the engine to the rotor (Fig. 1). Shafts made from AISI 4140 steel, which is quenched and tempered, generally exhibit high mechanical strength and toughness. However, failures in these shafts can lead to unexpected production stops, resulting in significant operational costs (He 2018).

1.3 Previous research on shaft failures

Limited research has been conducted on the fracture mechanisms of centrifugal pump shafts, particularly in mining applications where dynamic loading is common. Previous studies have addressed general fatigue behaviors and the impact of microstructure on shaft performance (Hua et al. 2023; Chan 2010). However, few works integrate a comprehensive analysis that combines fatigue behavior, crack growth, and microstructural analysis with finite element simulations to assess stress distribution in centrifugal pump shafts.

1.3.1 Research gap

Most existing investigations do not consider the combined effects of mechanical, microstructural, and numerical simulation factors in a single study to evaluate failures in centrifugal pump shafts under mining conditions. This gap limits the understanding of failure mechanisms and the effectiveness of specific preventive measures for industrial applications, highlighting the necessity of this research.

The field of centrifugal pump failure analysis has focused on understanding individual mechanisms like fatigue behavior, material properties, and stress factors (Hua et al. 2023; Zangeneh et al. 2014). However, research often remains fragmented, examining these factors in isolation rather than exploring their interactions under real-world mining conditions (Liu et al. 2019; Meysami et al. 2010).

This study was designed to fill that gap by integrating experimental testing, microstructural analysis, and numerical simulation, providing a holistic view of shaft failures. The approach reflects a logical progression from identifying key factors in the literature to replicating their interactions, aiming to improve maintenance strategies and extend equipment lifespan.

1.4 Research problem and objective

Given the significant downtime caused by shaft failures and the limited literature on comprehensive fracture analysis in this context, this study aims to investigate the causes of fracture failure in an AISI 4140 steel centrifugal pump shaft used in iron ore slurry processing. The research involves chemical composition analysis, mechanical testing, microstructural characterization, fatigue analysis, and finite element simulation to identify failure mechanisms and suggest preventive measures.

1.5 Problem theory

In a fatigue-loading scenario, the presence of material discontinuities is considered. Two criteria are used to evaluate the crack growth potential: the energy criterion (Griffith energy, G) and the resistance limit criterion (stress intensity factor, K_I). The energy associated with a crack is represented by G, as described in Eq. 1.

$$G = (\pi \cdot \sigma^2 \cdot a)/E \tag{1}$$

where σ is the applied stress, a is the crack size (discontinuity), and E is the Yang module.

According to the resistance limit criterion, for a crack, there is a stress intensity factor K_I that can be determined by Eq. 2.

$$K_I = \sigma(\pi \cdot a)^{1/2} \tag{2}$$

For both criteria, there are critical values G_c and K_{IC} for a crack to occur. These critical values can be determined by Eqs. 3 and 4, in which σf and ac correspond, respectively, to the critical failure stress and critical failure size.

$$G_c = (\pi \cdot \sigma_f^2 \cdot a_c)/E \tag{3}$$

$$K_{IC} = \sigma_f(\pi \cdot a_c)^{1/2} \tag{4}$$

By combining these two criteria, Eq. 5 can be reached.

$$G_c = (K_{IC})^2/E \tag{5}$$

K_{IC} is the fracture toughness of the material. Fracture toughness, or resistance to fracture, is a mechanical property of a material that measures its ability to resist the propagation of cracks. Its determination is made through tests. A high K_{IC} indicates that the material is less prone to crack propagation (Anderson 2017).

The literature includes a limited number of studies with cases similar to those in the present work, which makes this topic even more relevant. This study aimed to analyze the

Fig. 1 Centrifugal ore slurry pump parts
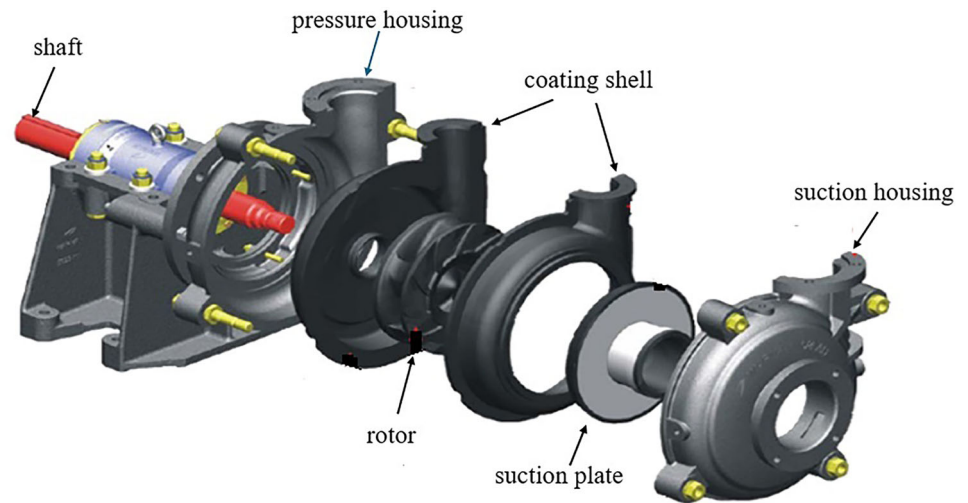
fracture failure of a centrifugal pump shaft through fatigue analysis, crack growth, microstructure, and material property analyses. This investigation contributes to understanding the causes of failures in centrifugal pump shafts and to the development of preventive measures in other industrial applications.

2 Experimental procedures

The experimental approach was designed to analyze the fractured centrifugal pump shaft through a series of tests, as described below:

2.1 Sample extraction and preparation

The fractured shaft, made of AISI 4140 steel, was disassembled, cleaned, and prepared for analysis. A sample was extracted from the fracture region, followed by surface cleaning with acetone for visual inspection, chemical analysis, and mechanical testing.

2.2 Mechanical testing

- *Tensile Tests:* Three specimens were prepared according to ASTM E8-21 standards, tested at a displacement rate of 5 mm/min using a 100 kN universal testing machine INSTRON (Model 2382, Instron, USA).
- *Hardness Tests:* Rockwell "C" (HRC) hardness tests were performed near the fracture site, following ASTM E18-20 standards using a Wilson hardness tester (Model 4 JR, Wilson Hardness, USA).
- *Impact Tests:* Charpy "V" notch impact tests were conducted on three specimens at 23 °C, in accordance with ASTM E23-18 using a Charpy Time JB300 impact

machine (Time Group Inc., China) using an EQUITECS testing machine (Model FR1, EQUITECS, Brazil). at room temperature.
- *Fatigue Tests:* Rotary bending fatigue tests were carried out following ASTM E466-15 standards, using a load ratio of $R = -1$ and a run-out of 3×10^6 cycles using a Time-Shijin testing machine (WDW-PWS series, Time Group Inc., China).

2.2.1 Reason for choosing stress ratio R = − 1

The stress ratio $R = -1R = -1$ was selected because it represents fully reversed loading, which is a common condition for shafts subjected to bending fatigue in real-world applications. This loading condition induces alternating tensile and compressive stresses, making it an ideal choice for evaluating the fatigue resistance of materials like AISI 4140 steel. It simulates the critical cyclic loading conditions experienced by the pump shaft during operation, providing a comprehensive assessment of its fatigue performance.

2.2.2 Crack growth tests

Conducted according to ASTM E647-15e1, using a prefabricated crack of 2.5 mm and a load ratio of $R = 0.1$.

2.3 Microstructural analysis

Samples from the fractured region were prepared for microstructural examination, which included sanding, polishing, and electrolytic etching with oxalic acid. Micrographs were obtained using scanning electron microscopy (SEM).

2.4 Finite element simulation

Numerical simulations were performed using the finite element method (FEM) to model stress distribution under static loading. The simulation considered a torque of 3885 Nm, shaft support by two bearings, and mesh quality criteria. The shaft was modeled using 3D geometry, and the mesh was generated with an element size of 5 mm, resulting in 136,274 nodes and 78,884 elements.

2.4.1 Jacobian ratio and mesh independence

The Jacobian ratio was determined by ensuring that the element quality remained within acceptable limits throughout the mesh, particularly in critical regions like the thread root. To validate mesh accuracy, a grid independence test was performed by refining the mesh incrementally and observing changes in the maximum stress values. The results showed minimal variation (less than 5%) between successive mesh refinements, indicating that the selected mesh size provided reliable results while maintaining computational efficiency. This approach ensured that the stress distribution analysis was not significantly influenced by mesh density, confirming the robustness of the FEM model.

2.4.2 Mesh selection and appropriateness

The choice of a 5 mm element size was based on balancing computational efficiency and result accuracy, focusing on capturing stress concentration details, particularly in the threaded region where the fracture occurred. Mesh quality criteria were carefully assessed to ensure proper element shape and convergence. This meshing approach allowed for an accurate representation of stress gradients while maintaining reasonable computation times, making it appropriate for analyzing the critical stress regions in this study.

3 Results and discussion

3.1 Visual analysis

As shown in Fig. 2a, b, shaft fractures occurred in the end region of the threaded region where the pump rotor was mounted, close to the thread exit radius. The shaft is equipped with a geometry that provides support in the pump casing through two rolling bearings located in the central region of the shaft. Through the shaft, torque is transmitted to the rotor inside the pump. In Fig. 13, the regions where the shaft bearings are located are highlighted in blue. On the side where the rotor is attached to the shaft, there is a 6.5 mm exit radius intended for the tool exit when machining the thread".

Visual analysis of the shaft fracture revealed a typical fatigue fracture, with several "ratchet marks" around the periphery of the fracture, as highlighted by arrows in Fig. 3a. Stable growth of the fatigue crack with a consequent reduction in the cross section was observed until it reached the final rupture region, as shown in Fig. 3a. The final rupture region represents approximately 46% of the cross section of the original region of the shaft before the crack. The presence of multiple "ratchet marks" suggested that the stress concentrator was strong. Failure occurs in the region where the thread ends close to its exit radius, where the highest stress values normally occur. The fractured shaft functioned for approximately 16 months before fracturing.

The thread root, as well as its exit radius surface, has a poor finish and deep machining scratches, which increase the probability of fatigue crack nucleation due to the increase in local stress concentration. In Fig. 3b, signs of crack nucleation can be observed at the bottom of the thread via liquid penetrant testing. A poor machining finish causes the concentration of stresses that contribute to the nucleation and consequent growth of the fatigue crack that culminates in the final fracture of the shaft. Threads are manufactured by machining. Poor finishing of the thread and the surface of the radius were observed only by visual analysis. The nucleation and propagation of fatigue cracks are strongly related to surface roughness (De Lacerda 2017).
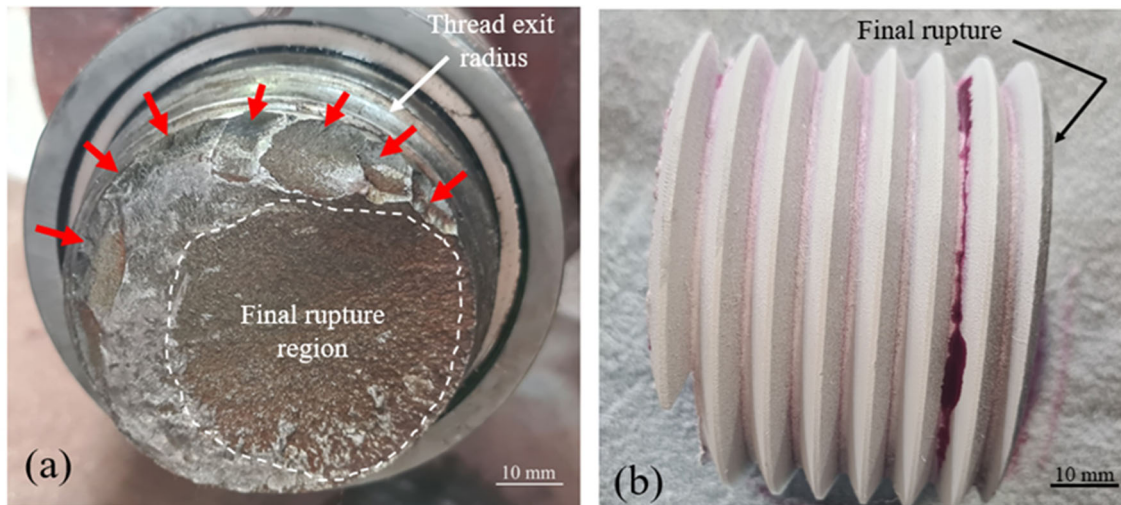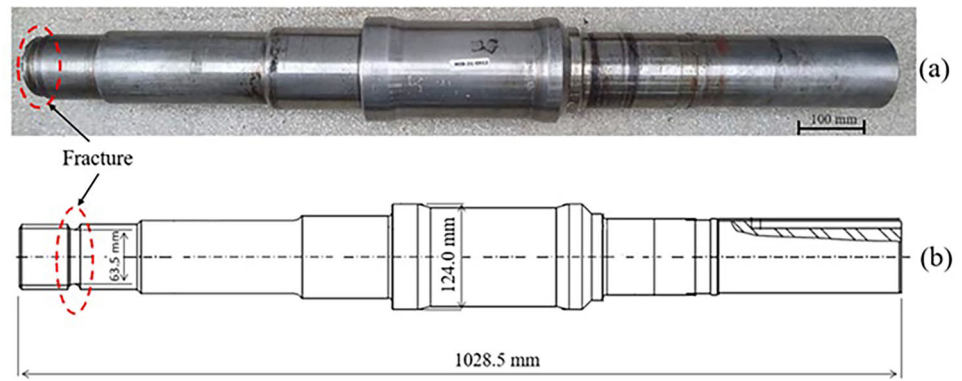
3.2 Chemical composition

Table 1 presents the chemical composition of the AISI 4140 steel used in the manufacture of the fractured shaft. The chemical analyses were performed using an optical emission spectrometer (OES) and evaluated according to the SAE AMS 6395J-2020 standard, ensuring that the testing methods align with recognized technical authorities for steel alloy characterization.

3.3 Microstructural analysis

During the quenching heat treatment, the steel is heated until it is austenitized and subsequently subjected to a continuous cooling process with a high cooling rate aimed at transforming the austenite into martensite. In this process, eventually, lower cooling rates may occur that favor the formation of phases other than martensite (for example, bainite) (Mendagaliev 2023).

As shown in Fig. 4, the AISI 4140 steel applied in the manufacture of the pump shaft under study presented a coarse and heterogeneous microstructure consisting of pearlite and bainite. The micrographs in Fig. 4a, b were obtained from the section perpendicular to the axial direction of the shaft. This type of microstructure is normally obtained when steel is subjected to high austenitization temperatures

Fig. 2 Centrifugal ore slurry pump shaft: **a** fractured shaft; **b** basic dimensions of the shaft

Fig. 3 Fractography of the AISI 4140 shaft: **a** fracture face; **b** cracked thread

Table 1 Chemical composition of AISI 4140 steel (% by mass)

Element	Measured composition (%)	Standard range (%) (SAE AMS 6395J-2020)
Carbon (c)	0.4	0.38–0.43
Silicon (Si)	0.2	0.15–0.35
Manganese (Mn)	0.88	0.75–1.00
Phosphorus (P)	0.015	≤ 0.035
Sulfur (s)	0.036	≤ 0.040
Chromium (Cr)	0.93	0.80–1.10
Molybdenum (Mo)	0.19	0.15–0.25
Iron	Bal	Bal

and then undergoes cooling at lower cooling rates. In this case, instead of forming martensite, austenite decomposes into bainite (supersaturated ferrite + cementite) (Pinedo 2021; Bhadeshia 2017). Normally, bainite can be classified according to two criteria: lower bainite that forms at lower

temperatures (250 to 400 °C) and upper bainite that forms at slightly higher temperatures (400 to 550 °C). The morphology of the upper bainite is presented as plate-like structures, and the lower bainite is presented as acicular structures, as highlighted in Fig. 4a, b (Singh 2021). The heat treatment probably did not result in a sufficiently high rate for the transformation of austenite into martensite, favoring the formation of bainite and pearlite (Mendagaliev 2023).

3.4 Tensile test

Figure 5 shows the engineering curve resulting from the average of the tensile tests carried out on 3 specimens of AISI 4140 steel used in the manufacture of the pump shaft under study. Table 2 lists the average tensile strength results of the tested AISI 4140 steel specimens.

The tensile test results (Table 2) align with standard values for AISI 4140 steel after quenching and tempering, indicating that the material retained expected tensile strength and ductility (ASTM E8-21). These results suggest that the heat treatment was generally effective in achieving the

Fig. 4 Microstructure of AISI 4140 steel (SEM)
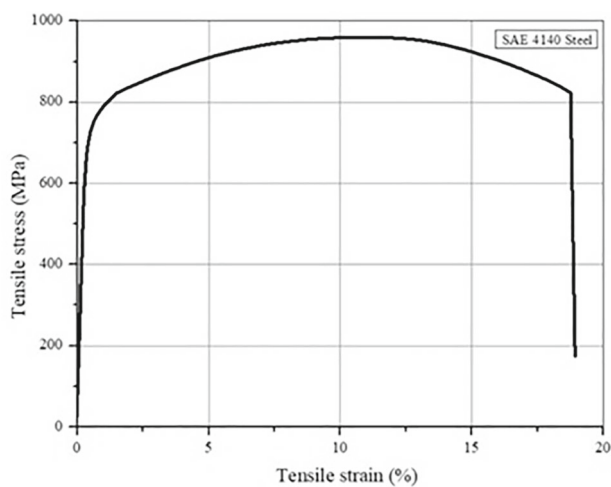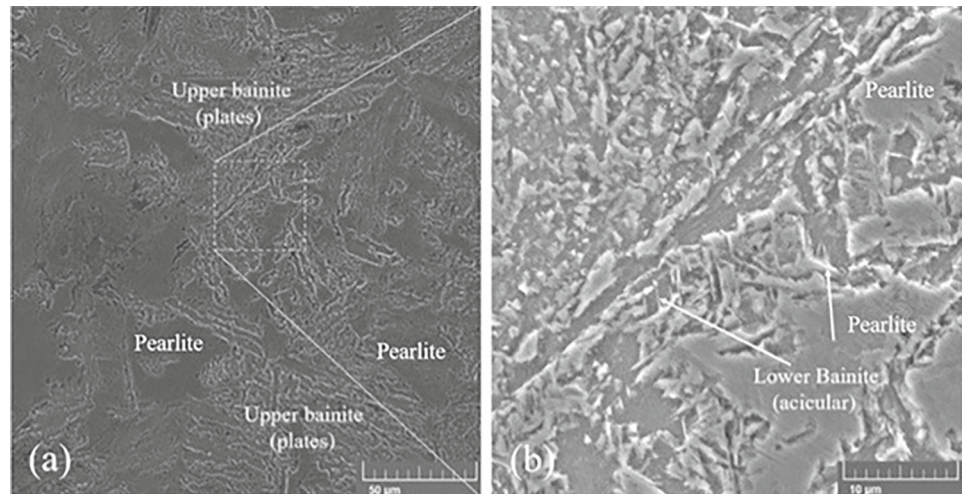
Fig. 5 Stress–strain engineering curve of AISI 4140 steel

**Table 2** Comparison of tensile test results with standard AISI 4140 values

Property	Tested specimen	Standard value	Reference
Ultimate tensile strength (MPa)	728 ± 12	655–1080	ASTM E8-21
Yield strength (MPa)	960 ± 19	415–710	ASTM E8-12
Elongation (%)	16 ± 2	15–25	ASTM E8-12

desired mechanical properties, consistent with previous findings (Senthilkumar & Ajiboye 2012).

According to the literature, the tensile properties of AISI 4140 steel can be modified via heat treatments. The tensile strength of heat treatable steels increases according to the following order of heat treatment: annealing > normalizing > quenching > tempering (Senthilkumar 2012; Badaruddin 2019). The tensile strength of the AISI 4140 steel specimens presented in Table 2 indicates that this steel was quenched and tempered. Quenching heat treatments followed by tempering improve the tensile strength while maintaining good toughness (Meysami 2010; Liu 2019).

As shown in Table 2, AISI 4140 steel exhibited high tensile strength with large longitudinal and transverse deformations. Figure 6a, b shows images of the tensile fracture of AISI 4140 steel, which reveal coherence between the morphology of the tensile fracture and its resistance and deformation results, as shown in Table 2. In Fig. 6a, referring to the central region of the tensile fracture, there is a predominance of dimples, indicating ductile behavior (the largest dimples are highlighted by arrows). Tensile fracture normally begins in the central region. These dimples result from the formation of coalesced microvoids, which initiate the tensile fracture process. Subsequently, the tensile failure continued to the edges of the material, where it began to present both dimples and cleavage planes, as shown in Fig. 6b. Cleavage planes indicate brittle behavior. Secondary cracks can also be observed in the tensile fracture of AISI 4140 steel. Secondary cracks are associated with brittle fracture by an intergranular mechanism. In contrast, cleavage is associated with brittle fracture by a transgranular mechanism (Hua 2023; Mandal 2022). Secondary cracks normally occur due to the existence of inclusions, chemical segregation, or preferential precipitation of phases at grain boundaries that occur during the thermomechanical processing of steel (Singh 2021). Spectroscopy (EDS). Thus, briefly, the tensile fracture pattern shown in Fig. 6c highlights the occurrence of manganese sulfide precipitation in the microstructure of AISI 4140 steel. The presence of manganese sulfide was observed by energy dispersive spectroscopy in AISI 4140 steel, which indicated that ductile and brittle fractures occurred in different regions.
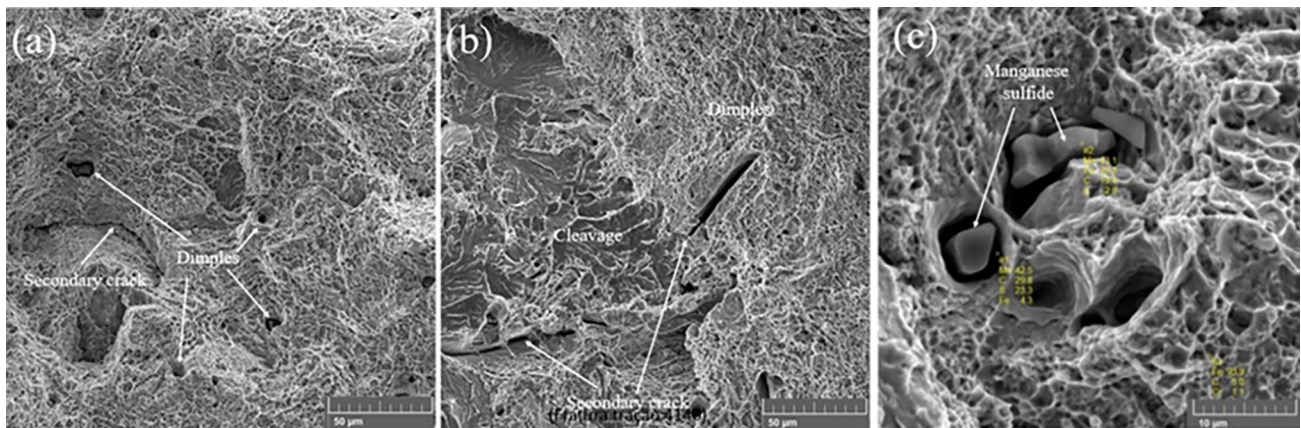
Fig. 6 Tensile fracture in AISI 4140 steel: **a** central region; **b** peripheral region; **c** manganese sulfide precipitation (SEM)

Under normal conditions, a body subjected to simple tension with static loading has its greatest stress initially occurring in the center of its cross section. Thus, in the case of materials that have ductile characteristics, fracture begins at the center of the cross section by the formation of microvoids that coalesce, giving rise to fracture in the presence of dimples. Cleavage may eventually occur due to transgranular fracture. (Anderson 2017).

3.5 Hardness test

Rockwell "C" (HR_C) hardness tests were carried out on a sample of AISI 4140 steel extracted from the fractured shaft, obtaining an average result of 29 ± 1 (5 tests). The hardness is directly correlated with the tensile strength and fatigue resistance of steel. The hardness can be improved by heat quenching, followed by tempering to increase the toughness (Mandal 2022; Anderson 2017).

A higher hardness hinders the formation of persistent slipping bands (PSBs) that occur when the material is subjected to dynamic loading. PSBs favor the appearance of intrusions and extrusions on the surface of the material, preferably in shear planes at 45°. These PSBs generate random stress concentration points on the surface of the material where fatigue cracks can nucleate and grow. According to De Lacerda (2017), the surface roughness of a material increases with the addition of PSBs, favoring stress concentrations during fatigue.

3.6 Impact test

Charpy impact tests were carried out on AISI 4140 steel samples extracted from the fractured shaft. The average impact energy absorbed was 9 ± 2 J, as shown in Table 3. Three specimens were tested at 23 °C. The low impact toughness obtained for AISI 4140 steel can be attributed to the coarse grains present in the impact microfractography image of the

**Table 3** Comparison of impact test results with standard AISI 4140 values

Property	Tested specimens	Standard values	Reference
Impact energy (J)	9 ± 2	12–27	ASTM E23-18
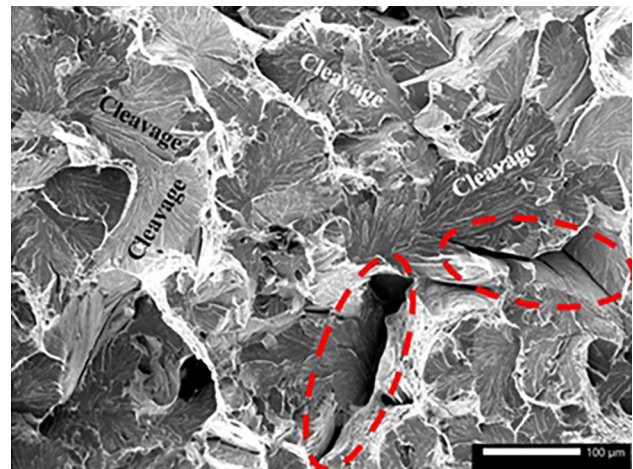
Fig. 7 Charpy impact microfractography (SEM) of AISI 4140 steel

steel, as shown in Fig. 7. The morphology of the Charpy impact fracture shown in Fig. 7 reveals the characteristics of a totally brittle fracture, as there is a predominance of cleavage (transgranular fracture) and secondary cracks, highlighted by red ellipses in Fig. 7 (intergranular fracture).

The impact test results (Table 3) showed lower energy absorption compared to standard AISI 4140 samples. This reduced impact toughness is likely due to the coarse bainitic microstructure observed, indicating potential deviations in cooling rates during heat treatment (Mendagaliev et al. 2023).
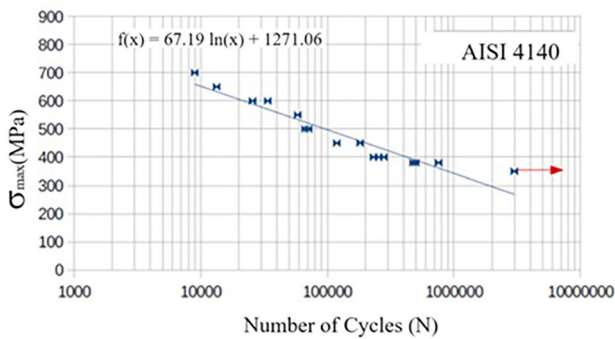
Fig. 8 Fatigue curve of the AISI 4140 steel

These findings highlight the importance of optimized heat treatment to improve toughness (Pinedo 2021).

The excessively coarse grain size of the microstructure of the AISI 4140 steel used in the manufacture of the shaft may have been caused by inadequate heat treatment. Most likely, the austenitization time and/or temperature were excessively high, favoring grain growth (Senthilkumar 2012; Meysami 2010; Chaouch 2018).

3.7 Fatigue test: SN curve

Figure 8 shows the SN curve of rotary bending fatigue tests carried out on AISI 4140 steel, whose specimens were extracted from the ore slurry centrifugal pump shaft, as previously reported. Fatigue tests were performed for up to 3×10^6 cycles, obtaining a fatigue limit of approximately 350 MPa for this value.

As shown in Fig. 9a, the fatigue fracture obtained by rotary bending testing of AISI 4140 steel reveals a predominance of brittle fracture (cleavage, river marks), even though there are small regions with ductile characteristics (small dimples). In Fig. 9b, secondary cracks are observed. Secondary cracks are generally formed due to intergranular grain detachment caused by the presence of inclusions in the grain boundaries that weaken the steel. These inclusions may be manganese sulfide (Fig. 6c). This type of secondary crack (intergranular crack) is more common in coarser structures (Chan 2010; Cheng 2019).

3.8 Crack growth: da/dN

Figure 10a, b shows the graphs of stable crack growth, da/dN, and the tested specimen of AISI 4140 steel extracted from the fractured shaft. From what can be seen, in the da/dN equation shown in Fig. 10a, the crack growth obeys the Paris law (Anderson 2017), with the parameters $C = 7.91^{-14}$ and $m = 4.25$. In this case, the crack growth rate increased linearly from approximately 4.7×10^{-9} m/cycle (4.7 nm/cycle) to 4.4

$\times 10^{-6}$ m/cycle (4.4 μm/cycle) in the range of ΔK varying from 10 to 60 MPa m$^{1/2}$.

The da/dN curve obtained for AISI 4140 steel shown in Fig. 10a was consistent with the behavior reported in the literature for this type of steel (Chan 2010; Cheng 2019). In this case, the hypothesis of any problem with steel in relation to its performance in this regard of stable fatigue crack growth is ruled out.

The growth of a fatigue crack occurs according to 3 distinct stages (I, II and III) depending on the amplitude, frequency and level of stress to which the material is subjected. Region I refers to the initial stage of unstable crack growth. In region II, the crack exhibits linear and stable growth behavior (Paris law); finally, in region III, the crack growth accelerates until the final fracture (Hua 2023).

3.9 Stress analysis via ANSYS

All of the discretization methods using the finite element method must comply with some mesh quality criteria. The quality of the mesh basically refers to the shape of the element, which comprises the relative dimensions between the base, height and width, and angles between faces or edges, among other characteristics. All shape checking criteria must be based on the relationship between the element in question and a reference element constructed with reference coordinates.

A static loading simulation of the shaft under study was carried out using the finite element method in ANSYS 2023 R1 software. According to the geometric data, the properties of AISI 4140 steel are indicated in Table 2, Young's modulus E = 205 GPa, Poisson's ratio = 0.29 and operational conditions of critical static loading (torque of 3885 Nm).

Figure 11 shows the design of the shaft under study, (a) modeled in 3D in the SpiceClaim software and (b) a detailed drawing of the shaft, in accordance with the original design dimensions and geometry.

For the simulation, the mesh was generated according to the following configuration: (a) physical preference: mechanical; (b) mesh element size: 5 mm; (c) number of nodes: 136,274; and (d) number of elements generated: 78,884. Figure 12 shows 3D images of the analysis mesh generated in the region of greatest interest, which is that of the thread and exit radius where the fracture occurred. The "equivalent tension" damage model was used for a "moment type" loading of 3885 Nm at the tip of the shaft. According to the analysis, this was the most critical point of the investigated element: 203.57 MPa on the axis with a radius of 6.5 mm and 214.77 MPa on the axis with a radius of 5.0 mm.

The finite element analysis (FEM) of the pump shaft was performed using ANSYS 2023 R1. The total computation time was approximately 45 min, with a mesh of 136,274 nodes and 78,884 elements. The simulation was conducted

Fig. 9 Microfractories of fatigue tests on AISI 4140 steel: **a** central region; **b** peripheral region (SEM)
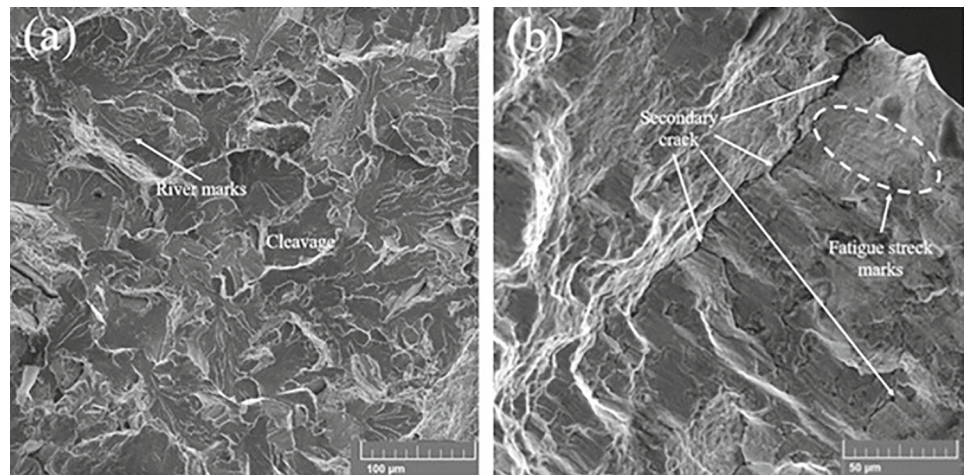
Fig. 10 Stable crack growth in AISI 4140 steel: **a** da/dN curve and **b** fractured specimen
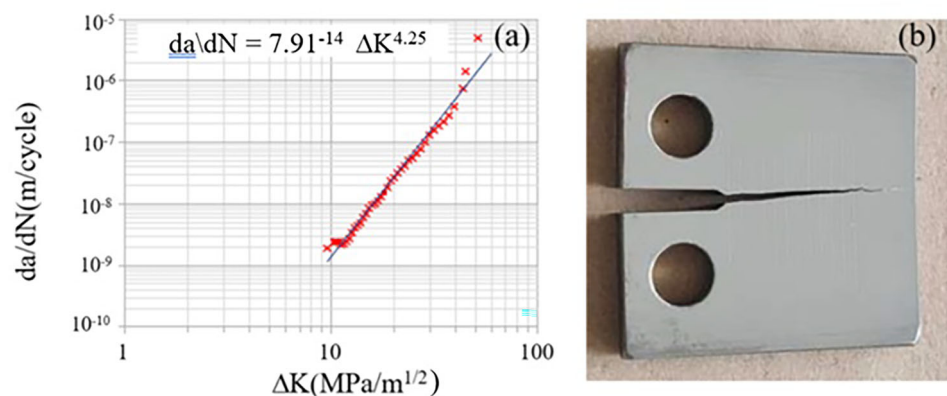
on a system with an Intel Core i7 processor and 32 GB of RAM. This computation time is typical for detailed 3D models of mechanical components and allowed for accurate stress distribution analysis.

Figure 13 shows the region where the bearings used to support the shaft are located. Then, a "cylindrical support" element was created in the bearing region, which simulates the sliding support of the shaft, as highlighted in blue in Fig. 13. The fixing and torque application locations at the ends of the shaft are also shown.

The simulation results are presented in Fig. 14a, where it is revealed that the critical stress concentration region is located at the tip of the shaft on the side of the thread that couples to the pump rotor, more specifically at the thread exit radius (Fig. 14b). At this location, the maximum Von-Mises equivalent stress (203.57 MPa) was produced in the shaft with a torque of 3885 Nm. It is important to note that the maximum stress was in the same location where the fracture occurred, as shown in Figs. 2 and 3.

There are several potential explanations for why failure might still occur under these load conditions. The following key factors are considered: (a) discrepancies between simulation and real-world conditions; (b) fatigue damage

accumulation; (c) unexpected loading or transient events; and (d) material defects or manufacturing issues. At the conclusion of the work, the reason for the failure that occurred in the case of the pump shaft studied in this work is more objectively demonstrated.

The finite element analysis (FEM) results in this study align with previous findings, such as Hua et al. (2023) and Chan (2010), which also reported stress concentration at the thread root under torque loading. However, unlike Zangeneh et al. (2014), who observed a more distributed stress pattern, our results show localized stress at the exit radius, likely due to specific shaft geometry and machining. Additionally, differences in crack growth rates, as discussed by Bhadeshia (2017), emphasize the influence of microstructure on fatigue behavior.

The loading conditions applied to the pump shaft, including both static and cyclic loads, play a significant role in the failure mode observed. The shaft experiences high torque during operation, which leads to stress concentration at critical points, particularly near the thread root and exit radius. This stress concentration is further exacerbated by cyclic loading, which promotes fatigue crack initiation and growth
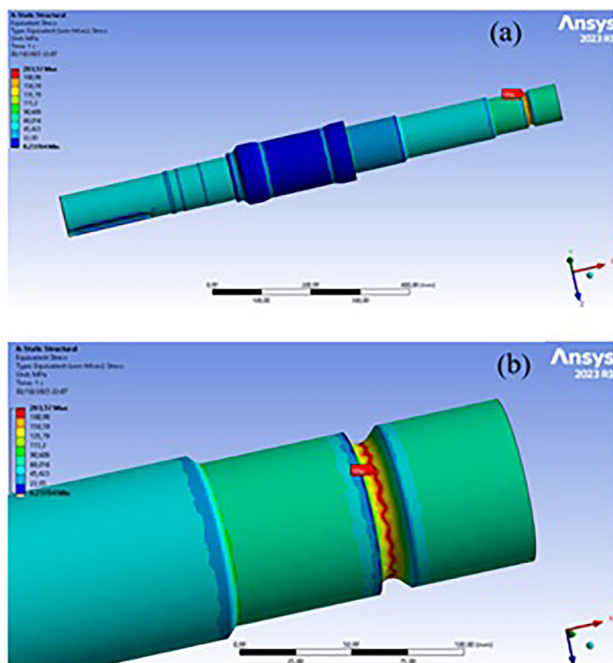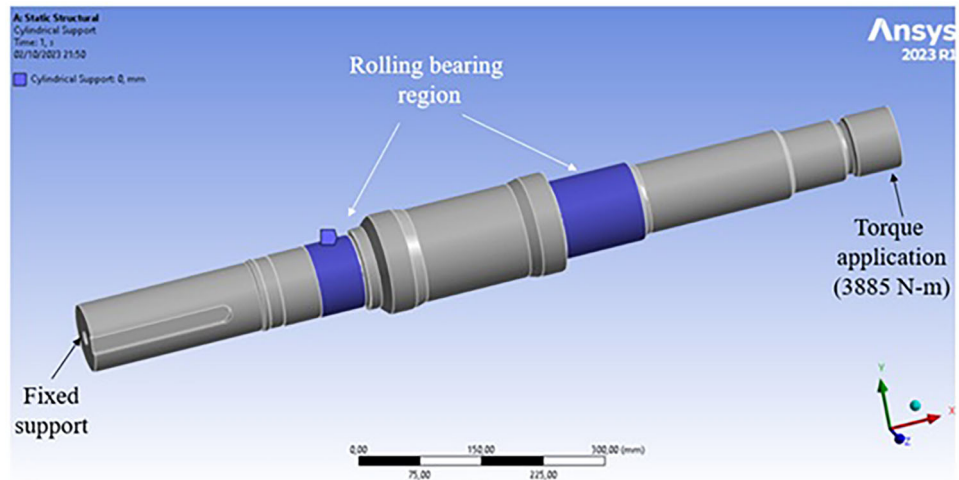
Fig. 11 **a** SpiceClaim 3D modeling of the shaft; **b** detailed drawing of the shaft
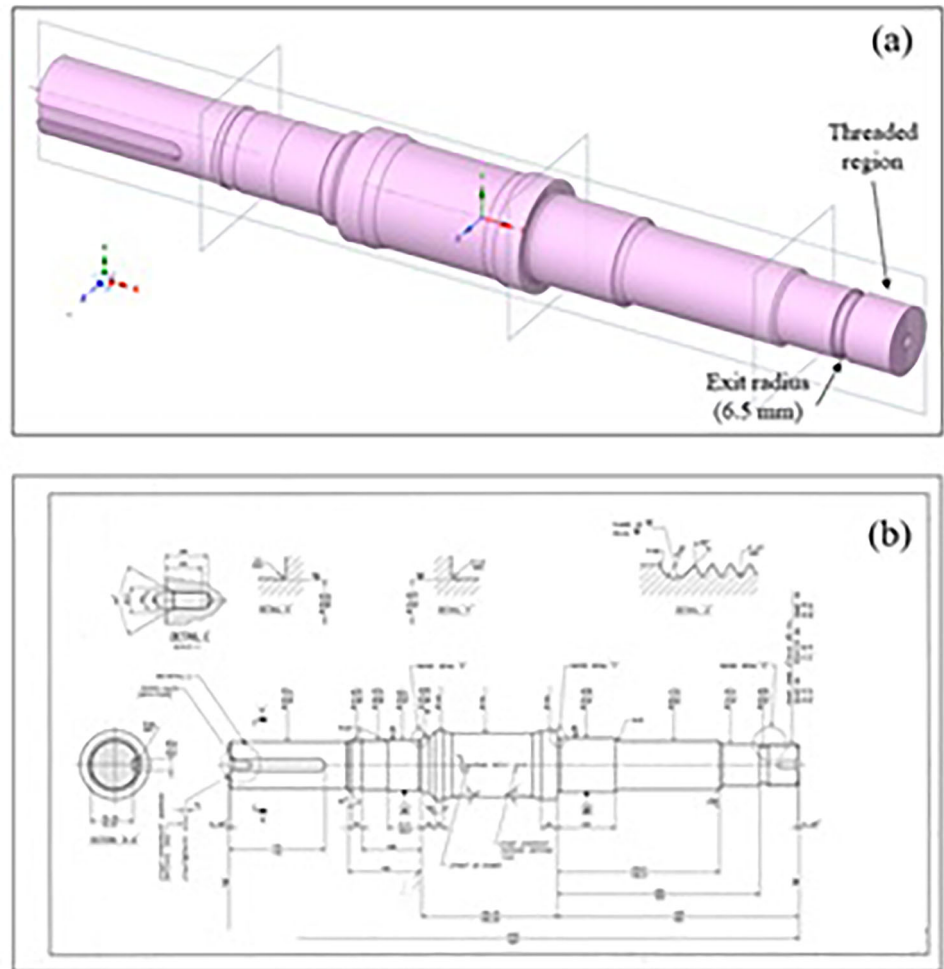
Fig. 12 Mesh for the numerical simulation of shaft loading
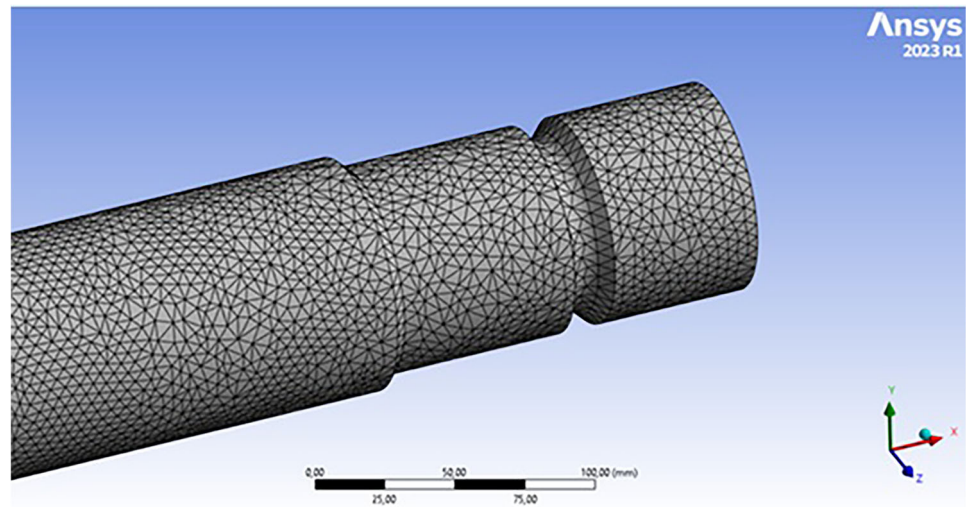
Fig. 13 Location of the rolling bearings, restriction, and torque application

Fig. 14 Distribution of simulated stresses in the shaft: **a** throughout the shaft; **b** in the critical region, tip of the shaft

over time. These practical loading conditions directly influence the shaft's fatigue resistance, highlighting the need for design improvements such as increasing the thread root radius and enhancing surface finish to mitigate stress concentration and improve durability in similar applications.

4 Correlations between the results and suggestions for preventive measures

It is known that failure due to fracture, which is typical of fractures occurring in the shaft of an iron ore centrifugal pump and is the subject of this work, does not occur due to a single cause. Typically, this type of failure occurs due to a combination of several factors. In the case of this work, such analyzed factors were associated with the results obtained by visual analysis of the fracture, microfractography, chemical composition of the steel and its mechanical properties (traction, hardness, impact, fatigue resistance) and mechanical stress analysis by numerical simulation charging.

According to Nan Hou (2022), shaft fatigue results from the progressive degradation of material due to cyclic stresses, attributable to various factors impacting shaft performance and lifespan. The main causes of fatigue failure include: improper design, material factors, common defects and improper assembly use, and maintenance, being in agreement with what was observed in this work.

According to visual analysis, shaft fracture occurred in the final region of the thread where the pump rotor was mounted, close to the thread exit radius (Figs. 2 and 3). The existence of multiple "ratchet marks" in the fracture suggested that there was a large concentration of stress in this region that led to the nucleation and propagation of fatigue cracks. The mentioned stress concentration was confirmed by numerical loading simulation analysis (Fig. 14).

Microstructural analysis revealed that the microstructure of the AISI 4140 steel applied in the manufacture of the pump shaft consisted of a mixture of pearlite and bainite. This type of microstructure is normally obtained when steel is subjected to high austenitization temperatures and then undergoes cooling at lower cooling rates, favoring the formation of these phases instead of martensite (Mendagaliev 2023), thus compromising the fatigue resistance of the steel. Another unfavorable microstructural aspect that can be observed is the large grain size of the microstructure shown in Fig. 7. This coarse grain reduces the impact resistance, favoring the propagation of transgranular cracks. The large

grain size may have been caused by inadequate heat treatment, which involved exposure to high temperatures for an excessive amount of time. The precipitation of manganese sulfide in the microstructure (Fig. 6) favored the embrittlement of the steel.

Briefly, considering the above, the following can be suggested as preventive measures to avoid failure occurring in the shaft under study: (a) minimize the stress concentration by using a larger radius at the thread exit; (b) increase the cooling rate in the quenching heat treatment to avoid exposing the steel for excessive time at high temperatures, aiming for a smaller grain size and formation of martensite instead of bainite and pearlite; and (c) use steel with lower sulfur content to minimize the precipitation of manganese sulfide in the microstructure.

5 Strengths and weaknesses of the analysis methods

5.1 Strengths

5.1.1 Comprehensive approach

The study employed a combination of experimental testing (visual analysis, tensile, hardness, impact, and fatigue tests) and numerical simulation (FEM), providing a robust understanding of the fracture mechanisms of the centrifugal pump shaft.

5.1.2 Detailed characterization

The characterization of AISI 4140 steel, including microstructural analysis and mechanical testing, offered valuable insights into the material's behavior under real operating conditions.

5.1.3 Finite element simulation

The FEM simulation effectively replicated real-world stress distribution, accurately identifying critical stress concentration points and supporting the overall analysis.

5.2 Weaknesses

5.2.1 Simulation limitations

The FEM analysis involved assumptions and simplifications, such as idealized boundary conditions and material properties, which may not fully represent the actual conditions of the pump shaft's operation.

5.2.2 Limited sample size

The study analyzed a single failed shaft, which may limit the generalizability of the findings. Analyzing additional samples could provide a broader perspective.

5.2.3 Surface quality influence

While poor machining finish was identified as a key factor, more advanced surface analysis (e.g., 3D profilometry) could offer a more detailed assessment of surface roughness and its effect on stress concentration.

6 Conclusion

This study presented a comprehensive analysis of the fracture failure of an AISI 4140 steel centrifugal pump shaft used in iron ore slurry processing. Visual inspection, mechanical testing, microstructural analysis, and finite element simulation identified fatigue as the primary failure mechanism, initiated at stress concentration points in the threaded region. The findings revealed coarse bainitic microstructure and manganese sulfide precipitates as factors contributing to reduced impact toughness and increased crack propagation.

The study's major contributions include:

- *Identification of key stress concentration points* through finite element analysis, matching the observed fracture location.
- *Microstructural characterization* highlighted inadequate heat treatment, resulting in bainite formation, which compromised fatigue resistance.
- *Recommendations for improved shaft design*, including increasing the root radius of threads, enhancing heat treatment processes, and reducing sulfur content to prevent manganese sulfide precipitation.

Limitations and recommendations for further studies

- *Single Specimen*: Analyzing a single shaft limits generalization; future studies should use a broader sample set.
- *Finite Element Modeling*: Idealized conditions may not fully capture real scenarios; future work should simulate more realistic operational loads.
- *Surface Roughness*: Advanced techniques, like 3D profilometry, could offer deeper insights into roughness and stress concentration.
- *Microstructure Scope*: Expanding the analysis beyond the fracture region could reveal more about overall fatigue resistance.

- *Loading Conditions*: Incorporating multi-axial loading would better represent operational stresses.
- *Environmental Factors*: Further studies should consider the impact of corrosion-fatigue in ore slurry environments.

Author contribution J.C. de Lacerda and W.D. dos Reis wrote the main manuscript. All authors reviewed the manuscript.

Data availability No datasets were generated or analysed during the current study.

Declarations

Conflict of interest The authors declare no competing interests.

References

Anderson TL (2017) Fracture mechanics: fundamentals and applications. CRC Press

Badaruddin M, Wardono H, Wang CJ, Rivai AK (2019) Improvement of low-cycle fatigue resistance in AISI 4140 steel by annealing treatment. Int J Fatigue 125:406–417. https://doi.org/10.1016/j.ijfatigue.2019.04.020

Bhadeshia H, Honeycombe R (2017) Steels: microstructure and properties. Butterworth-Heinemann

Chan KS (2010) Roles of microstructure in fatigue crack initiation. Int J Fatigue 32(9):1428–1447. https://doi.org/10.1016/j.ijfatigue.2009.10.005

Chaouch D, Sadok A, Bendaoudi SE, Chaouch A (2018) Effect of charpy impact test on microstructure properties of AISI4140 steel. Mech Mech Eng 22(4):1463–1469

Cheng A, Chen NZ, Pu Y (2019) An energy principles based model for fatigue crack growth prediction. Int J Fatigue 128:105198. https://doi.org/10.1016/j.ijfatigue.2019.105198

De Lacerda JC, Martins GD, Signoretti VT, Teixeira RLP (2017) Evolution of the surface roughness of a low carbon steel subjected to fatigue. Int J Fatigue 102:143–148. https://doi.org/10.1016/j.ijfatigue.2017.05.010

He R, Dai Y, Lu J, Mou C (2018) Developing ladder network for intelligent evaluation system: Case of remaining useful life prediction for centrifugal pumps. Reliab Eng Syst Saf 180:385–393. https://doi.org/10.1016/j.ress.2018.08.010

Hou N, Ding N, Qu S, Guo W, Liu L, Xu N, Tian L, Xu H, Chen X, Zaïri F, Wu CM (2022) Failure modes, mechanisms and causes of shafts in mechanical equipment. Eng Failure Anal 136:106216. https://doi.org/10.1016/j.engfailanal.2022.106216

Hua M, Cao C, Cai Y, Ge J, Zhong F, Mao J (2023) Failure analysis and structural fatigue resistance design of multistage centrifugal pump shaft. Eng Fail Anal 153:107545. https://doi.org/10.1016/j.engfailanal.2023.107545

Liu Y, Lian Z, Xia C, Qian L, Liu S (2019) Fracture failure analysis and research on drive shaft of positive displacement motor. Eng Fail Anal 106:104145. https://doi.org/10.1016/j.engfailanal.2019.08.011

Mandal SK, Shekh MI, Kumar S, Chakraborty A, Kumar N (2022) Failure analysis of PTO shaft of an agricultural tractor. Mater Today Proc 66:3924–3929

Mendagaliev RV, Ivanov SY, Babkin KD, Lebedeva NV, Klimova-Korsmik OG, Turichin GA (2023) Influence of the thermal cycle on microstructure formation during direct laser deposition of bainite-martensitic steel. Mater Chem Phys 300:127523. https://doi.org/10.1016/j.matchemphys.2023.127523

Meysami AH, Ghasemzadeh R, Seyedein SH, Aboutalebi MR (2010) An investigation on the microstructure and mechanical properties of direct-quenched and tempered AISI 4140 steel. Mater Des 31(3):1570–1575. https://doi.org/10.1016/j.matdes.2009.09.040

Pinedo CE (2021) Tratamentos térmicos e superficiais dos aços. Blucher, Brazil

Rodrigues AFDV, Junior HD, Silva K, Zhou J, Galvin KP, Filippov LO (2023) Transforming iron ore processing–Simplifying the comminution and replacing reverse flotation with magnetic and gravity separation. Miner Eng 199:108112. https://doi.org/10.1016/j.mineng.2023.108112

Senthilkumar T, Ajiboye TK (2012) Effect of heat treatment processes on the mechanical properties of medium carbon steel. J Miner Mater Charact Eng 11(2):143–152

Singh S, Samir S, Kumar K, Thapa S (2021) Effect of heat treatment processes on the mechanical properties of AISI 1045 steel. Mater Today Proc 45:5097–5101. https://doi.org/10.1016/j.matpr.2021.01.590

Zangeneh S, Ketabchi M, Kalaki A (2014) Fracture failure analysis of AISI 304 L stainless steel shaft. Eng Fail Anal 36:155–165. https://doi.org/10.1016/j.engfailanal.2013.09.013